Journal of Environmental Management xxx (xxxx) xxx

Contents lists available at ScienceDirect

Journal of Environmental Management

journal homepage: http://www.elsevier.com/locate/jenvman

Research article

Granulation and calcination of alum sludge for the development of a phosphorus adsorbent: From lab scale to pilot scale

Maarten Everaert [a,*], Jef Bergmans [a], Kris Broos [a], Benjamin Hermans [b], Bart Michielsen [a]

[a] Unit Sustainable Materials Management, Flemish Institute for Technological Research (VITO), Boeretang 200, 2400, Mol, Belgium
[b] De Watergroep, Vooruitgangstraat 189, 1030, Brussels, Belgium

ARTICLE INFO

Keywords:
Alum sludge
Calcination
Drinking water production
Granulation
Phosphorus adsorption
Water treatment

ABSTRACT

Alum sludge, an Al-oxyhydroxide rich waste product from water treatment practices, has the potential to be valorized as a P adsorbent material. However, several challenges currently prevent its application as an adsorbent in industrial setting, *i.e.* a limited P adsorption capacity due to saturation by organic matter and a fine nature resulting in percolation problems in adsorption bed setups. In this study, granulation and subsequent calcination of alum sludge were proposed to overcome these issues and to improve the P adsorption properties of alum-based adsorbent (ABA) materials. The effect of calcination temperature on the physicochemical properties of granular material was examined using X-ray diffraction, mass-spectroscopy coupled thermogravimetric analysis, Fourier-transform infrared spectrometry and specific surface area analysis, combined with density and crushing strength measurements. The ABA material obtained at 550 °C showed superior P adsorption properties and, therefore, this material was selected for further P adsorption testing and characterization (scanning electron microscopy and sieving). Batch P adsorption tests showed that this material had a maximum P adsorption capacity of 7.27 mg-P g^{-1}. Kinetic adsorption tests determined the effect of the solid-to-liquid ratio and the granule particle size on the P removal. Finally, the performance of the ABA-550 material was tested in a pilot-scale adsorption setup, using a surface water stream (0.47 mg-P L^{-1}) at a flow rate of 200 L h^{-1}. During the test, the P removal efficiency always exceeded 86%, while the material maintained its structural stability. The results of this study illustrate the potential of granulated/calcined ABA materials for P adsorption, paving the way for the industrial application of this novel, sustainable P removal technology.

1. Introduction

The popularity of mineral phosphorus (P) sources during the past decades heavily magnified the P concentrations in sidestreams, such as wastewater and drainage water. As a result, improper treatment of industrial/domestic wastewater and leaching/runoff of P from agricultural fields can lead to significant losses of P to the environment (Desmidt et al., 2015; Djodjic et al., 2004; Mcdowell et al., 2001). Elevated P levels in surface waters are known to be one of the main driving forces of eutrophication in aquatic ecosystems and, therefore, the reduction of the P load in wastewater or drainage water is necessary to warrant the quality of the aqueous environment (Carpenter, 2008).

Adsorption technology is a very useful tool to capture P from aqueous waste streams: it allows the treatment of large volumes in continuous operations and can reach low effluent P concentrations (Kumar et al., 2019). So far, many engineered P adsorbents have been developed, including magnetic oxide nanoparticles (Yoon et al., 2014), modified zeolites (Yang et al., 2015), pyrolyzed biochar (Kizito et al., 2017) and layered double hydroxides (Dox et al., 2019; Seftel et al., 2018). However, a cost-effective application of these materials on an industrial scale, given the immense volume of aqueous streams requiring P removal treatment, is questionable. Therefore, adsorbent development based on cheap and abundant raw materials, such as secondary raw materials and residue streams, is gaining a lot of attention.

In the process of drinking water production, aluminium salts (*e.g.* $Al_2(SO_4)_3$ or $AlCl_3$) are commonly added to reservoir water to initiate the coagulation of natural organic matter (NOM). The dissolved Al forms complexes with the NOM molecules, which strongly reduces the solubility of NOM and results in the formation of solid coagulated material. The obtained material after coagulation, sedimentation and centrifugation, often referred to as alum sludge, can be perceived as a waste product of drinking water production. With an estimated global

* Corresponding author.
E-mail address: maarten.everaert@kuleuven.be (M. Everaert).

https://doi.org/10.1016/j.jenvman.2020.111525
Received 3 June 2020; Received in revised form 13 October 2020; Accepted 19 October 2020

production exceeding 10,000 ton y^{-1}, alum sludge is one of the largest by-products generated by water processing industries (Ahmad et al., 2016). Over the past two decades, a possible valorization route has been explored for this waste stream: alum sludge can be used as a low-cost alum-based adsorbent (ABA), since the high aluminium content of these materials allows efficient removal of dissolved pollutants such as F, Pb, As, Se, Cr, Hg and P (Hovsepyan and Bonzongo, 2009; Ippolito et al., 2009; Jeon et al., 2018; Jung et al., 2016; Kim et al., 2020; Li et al., 2018; Sujana et al., 1998; Zhou and Haynes, 2011). The ABA materials are capable of strongly binding phosphate anions via the formation of inner-sphere complexes (Yang et al., 2006b). With P being often abundantly present in wastewater, reservoir water or surface water, P removal from those streams is likely one of the most promising valorization strategies for sludge-derived materials (Dassanayake et al., 2015).

Several research studies investigated the potential of alum sludge as a P adsorbent, and explored how the P adsorption is affected by the solution pH (Kim et al., 2002; Maqbool et al., 2016; Yang et al., 2006a), incubation time (Babatunde and Zhao, 2010; Wang et al., 2011), alum sludge aging (Yang et al., 2008), P source speciation (Babatunde et al., 2008; Kim et al., 2002) and competition for sorption with other common wastewater compounds (*e.g.* SO_4^{2-}, Cl^- and NOM) (Georgantas and Grigoropoulou, 2005; Kim et al., 2002; Yang et al., 2006b). The maximum P adsorption capacity reported in these studies varied strongly (3.5–23.0 mg-P g^{-1}), which is likely the result of a broad range in Al content of the different alum sludge materials. Furthermore, Zhao and Zhao (2009) and Zohar et al. (2017) investigated a subsequent P desorption from ABA materials, aiming at the recycling of desorbed P and reuse of the ABA materials.

The P adsorption technology with ABA materials is very promising, yet several challenges currently prevent alum sludge to be valorized as a performant P adsorbent material in an industrial setting. Firstly, untreated alum sludge has a limited P adsorption capacity and has been linked to risks of NOM leaching from the material during P adsorption (Liu et al., 2016). These problems can be overcome by the calcination of the alum sludge, which results in the degradation of NOM and lowers the competition for P sorption sites (Tie et al., 2013). Secondly, alum sludge is typically a fine material, with particle sizes below 300 μm (Dayton and Basta, 2005). The use of a powdered ABA material in fixed-bed adsorption filter systems, however, results in a large pressure drop and is associated with a high risk of clogging. Therefore, several approaches for the development of granular sludge-based adsorbents have recently been explored. Babatunde et al. (2010) and Yang et al. (2006a) used air-dried granular material for P removal, but this resulted in a high risk of granule disintegration. Granular ABA materials have also been prepared via the treatment of powdered sludge in a Na/Ca alginate dispersion (Jung et al., 2016; Kang et al., 2019). This resulted in a slight reduction of the P adsorption capacity, but also in a decrease of harmful metal leaching (*e.g.* Al, Cr, Ni, Pb, Zn) from the alum sludge (Li et al., 2018). Finally, also the sintering of mixtures of sludges with residues or additives (fly ash, oyster shell, clay, sodium silicate) has been tested for the development of a granular ABA material (Cheng et al., 2018; Shen et al., 2018; Xu et al., 2008).

In this study, these recent trends of granulation and calcination of alum sludge were combined for the development of a P adsorbent material. Alum sludge material, recovered from a drinking water production center located in Kluizen (Belgium), was granulated and subsequently calcined at different temperatures. The effect of the calcination temperature on the physicochemical properties and P adsorption efficiency of the granulated material was explored. One performant calcined granulated alum sludge material was selected based on an initial P adsorption test, of which the adsorption capacity and kinetics were determined in synthetic P solutions. Finally, this material was tested for its P removal efficiency in pilot-scale adsorption column for 24 h (32.5 kg adsorbent, 200 L h^{-1}) for the treatment of surface water from the water catchment area of The Blankaart, Belgium. The results of this study warrant P adsorption with ABA materials to be a viable new technology to remove P from aqueous streams on an industrial scale.

2. Material and methods

2.1. Sampling and characterization of sludge material

The alum sludge was sampled at the water production center located in Kluizen, Belgium. Here, $AlCl_3$ was used as a flocculating agent in the treatment of reservoir water. The obtained sample was dried at 100 °C to constant weight (*Vötsch VTU 100/150*, Balingen, Germany).

The chemical composition of the alum sludge was determined by inductively coupled plasma atomic emission spectroscopy (ICP-OES) and X-ray fluorescence analysis. The ICP-OES analysis was performed with a *PerkinElmer Avio 500* with *Elemental Scientific prepFAST* autosampler after microwave digestion in $HCl/HNO_3/HBF_4$ for 2 h at 105 °C. For the XRF analysis, the alum sludge was first calcined at 1000 °C for 4 h in a muffle furnace (*Thermolyne*, Iowa, USA). From the obtained ashes, smelt beads were prepared by mixing the ashes with $Li_2B_4O_7$ at a sample/$Li_2B_4O_7$ mixing ratio of 1/10 and fusing the mixture in an automatic fusion system (*XrFuse 2, XRF Scientific*, Brussels, Belgium) at 1250 °C for 11 min. The obtained smelt beads were characterized with an energy dispersive X-ray fluorescence (XRF) spectrometer (*He XEPOS* instrument, *Spectro Analytical Systems*, Kleve, Germany) equipped with a 50 W tungsten end window tube (max. 60 kV, 2 mA) and a Silicon Drift Detector. Additionally, thermal treatment of the sludge at 1000 °C for 4 h was used to determine the loss on ignition (LOI).

Using mass spectroscopy coupled thermogravimetric analysis (TGA-MS, *Netzsch STA449 C Jupiter*, Selb, Germany), the thermal behavior of the raw sludge material was determined. For this analysis, 50 mg of powder was placed in an alumina crucible and heated from 30 °C to 1050 °C with a heating rate of 10 °C min^{-1} under an airflow of 50 mL min^{-1}. The setup had an integrated quadrupole mass spectrometer (*Netzsch TGA/STA-QMS 403 D Aëolos*, Selb, Germany) to simultaneously follow the generated gasses as the powder is heated, which allowed the weight loss obtained from TGA curve to be related to the decomposition of various phases.

2.2. Preparation and characterization of the ABA granular material

The dried alum sludge was reduced in size to below 4 mm using a disc mill (*Retsch* Disc Mill DM 200, Haan, Germany). The resulting material was classified and the fraction between 1 and 4 mm was retained. The 1–4 mm fraction was treated in a furnace (*Nabertherm LH 60/14*, Lilienthal, Germany) for 2 h at either 100 °C, 200 °C, 300 °C, 400 °C, 500 °C, 550 °C or 600 °C, obtaining ABA materials referred to as ABA-100, ABA-200, ABA-300, ABA-400, ABA-500, ABA-550 and ABA-600, respectively.

The crystallographic properties of the prepared ABA granules were investigated by X-ray diffraction (XRD) on the powders obtained after milling granular materials. The XRD patterns were recorded on a *PANalytical X'Pert PRO MPD* diffractometer with filtered CuKα radiation. Measurements were done in the 2θ mode using a bracket sample holder with a scanning speed of 0.04° s^{-1} in continuous mode. The crushed granules were analyzed by attenuated total reflection Fourier-transform infrared (ATR-FTIR) spectroscopy (*Nicolet-Nexus, Thermo*, USA). The data processing of the obtained spectra was performed using *OMNIC* software. The specific surface area of powdered ABA materials was measured using a *Quantachrome Nova 3000* instrument with the Brunauer-Emmett-Teller (BET) N_2 sorption theory. The materials were pre-treated by degassing at 40 °C under N_2 atmosphere for 16 h. The density of the powdered ABA materials was measured using a *Micromeritics Accupyc II 1340* Helium pycnometer. Approximately 2 g of these powders was used to carry out the measurement. Morphological observations and observations on the elemental distribution in powdered ABA-550 material were carried out using a scanning electron microscope (SEM) *FEI NOVA NANOSEM 450* with EDX analyzer *BRUKER*

QUANTAX 200 with SDD detector.

The crush strength of granular ABA materials was determined via single-granule compressive measurements using an *Instron 5582 Universal* testing bench. The maximal load during all measurements was set to 1 kN, while the frame speed was 0.5 mm min^{-1}. The final compressive strength (in MPa) was estimated by the *Bluehill* 3 software, considering the diameter and measured compressive strength (in N). The load tests were performed on one single aggregate at a time, and were repeated for 10 granules per sample.

The particle size distribution of the ABA-550 material was determined by sieving the sample at 1.0, 1.12, 1.4, 2.0, 2.5, 3.35 and 4 mm using a sieve tower setup. The gravimetric measurement of each fraction was used to obtain the particle size distribution curve.

2.3. P adsorption experiments

2.3.1. Adsorption capacity

The P adsorption properties of the ABA-100, ABA-300 and ABA-550 granular materials were explored by assessing their P adsorption from synthetic 100 mL solutions of 33 mg-P L^{-1} with a varying initial pH between 4 and 9. The P solutions were prepared by dissolving KH_2PO_4 in distilled water, and diluted HCl or NaOH solutions were added to adapt the pH. For 24 h, suspensions with a S:L ratio of 10 g L^{-1} were shaken at 20 °C. After this period, the pH of the solutions was measured again, and the solutions were sampled and filtered (*chromafil® RC-45/25 – 0.*45 µm). The filtered samples were measured by inductively coupled plasma atomic emission spectroscopy (ICP-OES, *PerkinElmer Avio 500* with *Elemental Scientific prepFAST* autosampler) to determine the P adsorption.

The P adsorption isotherm of the ABA-550 material was determined by incubating this material (S:L ratio of 10 g L^{-1}) for 24 h at 20 °C in solutions with P concentrations ranging between 1.5 and 160 mg-P L^{-1}. The initial solution pH was brought to 7.0. After the reaction, the pH and P concentration of the solutions were measured. The obtained adsorption isotherm data were fitted to the Langmuir isotherm model (Eq. (1)) and the Freundlich isotherm model (Eq. (2)) (Freundlich and Hatfield, 1926; Langmuir, 1932).

$$q = \frac{q_m k_L C}{1 + k_L C} \tag{1}$$

$$q = k_F C^{\frac{1}{n}} \tag{2}$$

2.3.2. Kinetics of P adsorption

The P sorption kinetics of the ABA-550 material was examined by incubating the sorbent in synthetic solutions of 1.6 mg-P L^{-1} at initial pH 7, focusing on the effect of i) the S:L ratio and ii) the ABA-550 particle size. The effect of the S:L ratio during adsorption was examined by varying the amount of ABA-550 added to the solution, *i.e.* S:L ratio of 2, 10 or 50 g L^{-1}. The effect of the ABA-550 particle size on P sorption kinetics was assessed by sieving the ABA-550 material over a 1 mm, 2 mm and 4 mm sieve, obtaining three samples with varying granule size (<1 mm, 1–2 mm and 2–4 mm) that were used for P adsorption at a S:L ratio of 20 g L^{-1}. At specific times after the start of adsorption, the solution was sampled for P analysis with ICP-OES. The obtained adsorption kinetic data were fitted to the pseudo-fist-order model (Eq. (3)), the pseudo-second-order model (Eq. (4)) and the intraparticle diffusion model (Eq. (5)).

$$q = q_e\left(1 - e^{-k_1 t}\right) \tag{3}$$

$$q = \frac{k_2 q_e^2 t}{1 + k_2 q_e t} \tag{4}$$

$$q = k_d t^{0.5} + C \tag{5}$$

2.4. Pilot-scale column study

In order to determine the performance of the ABA-100 particles and ABA-550 particles under more realistic conditions, a test under dynamic conditions was performed on the water of the buffer basin (63 ha) of the drinking water production center "De Blankaart" operated by *De Watergroep* (Fig. 1a). This buffer basin extracts water from a surface water area of 25,000 ha in the drainage basin of the river Yser and the polders of nature reserve De Blankaart. The treatment plant has a production capacity of 60,000 m^3 of drinking water per day, providing water for 315,000 users. Due to water quality issues (*e.g.* high phosphate concentrations) of surface water sources for the buffer basin, no water can be added to the basin from April until September to avoid algae growth. The use of an adsorption system based on ABA material to treat surface water before entering the basin could be a solution to avoid high P concentrations (aiming at 0.033 mg-P L^{-1}), thereby providing more water security during the summer months.

To perform this test, a self-designed flexible pilot installation was built (details in Figure S1). It consists of three down-flow columns (diameter 40 cm, height 150 cm), which can be either operated in a parallel or serial mode (Fig. 1b). The flow is controlled by adapting the height of the water level in the column above the ABA materials and can vary between 50 and 1000 L h^{-1}. Online measurements of flow rate, pressure, pH and NTU were performed for continuous monitoring (Fig. 1c and d). The columns were filled with 32.5 kg of the ABA material, either ABA-100 or ABA-550. A flow of 200 L h^{-1} of unfiltered water was used, resulting in a contact time of approximately 10 min. The experiment was performed on 6 and August 7, 2018, because at this time the water in the basin contained a relatively high P amount of 0.43 mg-P L^{-1}. The water temperature that time was 24.1 °C. For 24 h, the P concentration of both the influent and the column effluent was sampled once every hour using an automated collection system. The total P concentration of these samples was determined via a spectrophotometric method (EN ISO 6878), using a Thermoreactor RD125 (*VWR International*) and a *Lovibond* MD 600 spectrophotometer.

3. Results and discussion

3.1. Alum sludge characterization

The sampled alum sludge, prior to granulation and calcination to ABA-materials, was characterized for its chemical composition and thermal behavior. From the XRF analysis (Table S1) and ICP-OES analysis (Table S2), comparable values were obtained for the Al content of the alum sludge. The determined Al_2O_3 content of 73.9% was relatively high compared to other alum sludges characterized in literature, whereas the SiO_2 content was relatively low (Kim et al., 2002, 2012; Maqbool et al., 2016). Also Ca (18 g kg^{-1}) and Fe (16 g kg^{-1}) were present in minor amounts. The loss of ignition (LOI) was 12.03%, which could be attributed to i) evaporation of physically sorbed H_2O, ii) evaporation of chemically sorbed H_2O and iii) thermal degradation of NOM.

The thermal behavior of the alum sludge was investigated with TGA-MS (Fig. 2a). A CO_2 loss was recorded between 200 °C–600 °C as a result of the degradation of NOM (Guo et al., 2016). For the H_2O loss, two distinct regions were identified: i) below 200 °C, H_2O loss was attributed to physically sorbed H_2O; ii) from 200 °C onwards, the NOM degradation and removal of chemically-sorbed H_2O contributed to the loss of H_2O. For the presented temperature range, no loss of SO_2 was recorded.

3.2. ABA material characterization

The ABA materials obtained after granulation and calcination were characterized using a range of techniques. With XRD analysis, the crystallographic properties of the ABA materials obtained at varying calcination temperatures were examined (Fig. 2b). At temperatures

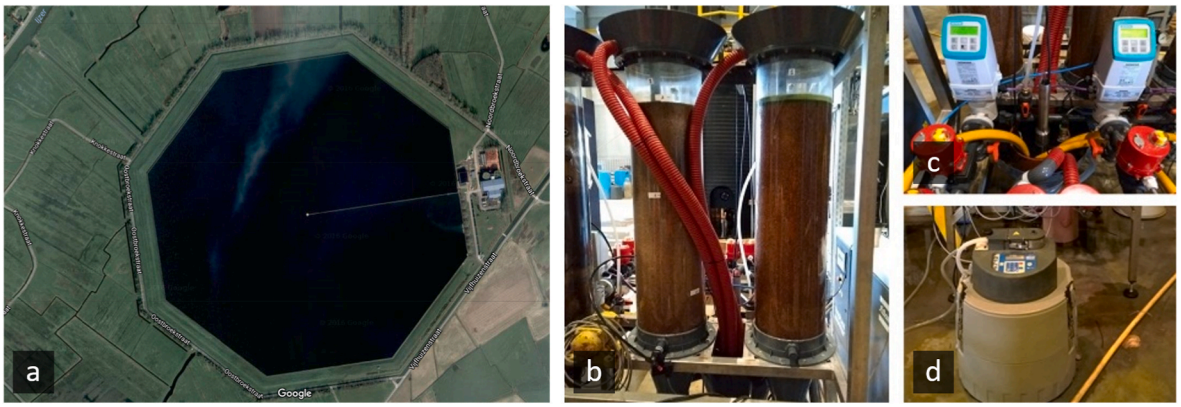

Fig. 1. Areal picture of the Blankaart reservoir (a), and pictures of the components of the pilot-scale setup: columns (b), turbidity meters (c) and sampling equipment (d).

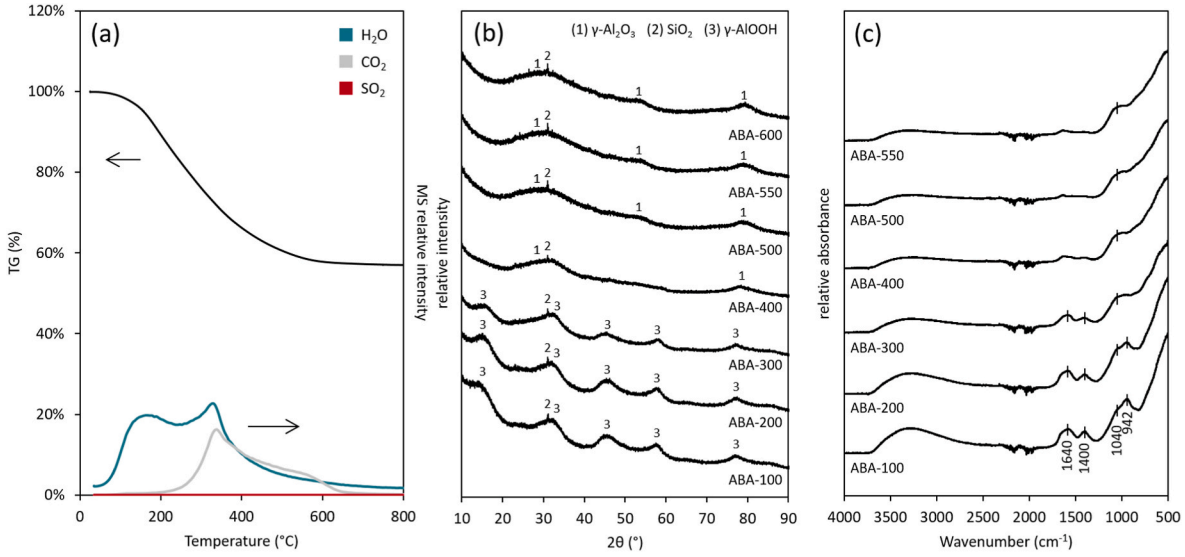

Fig. 2. TGA-MS characterization of the alum sludge (a), and XRD patterns (b) and ATR-FTIR spectra (c) of the thermally-treated granulated alum sludge.

below 400 °C, boehmite (γ-AlOOH) was the most prominent mineral phase. From 400 °C onwards, the boehmite phase completely transformed to γ-alumina (γ-Al_2O_3) (Igor Levin and David Brandon, 1998). Dehydration associated with this phase transition confirmed the contribution of the H_2O loss recorded with TGA-MS (Fig. 2a). In all XRD patterns, the characteristic (111) reflection of quartz (SiO_2) was present. With XRF, a SiO_2 content of 11.1% was measured in the fresh alum sludge, which likely remained stable as a quartz phase at all tested calcination temperatures.

The functional groups of the calcined materials were characterized using ATR-FTIR (Fig. 2c). For all materials, a band was shown around 3290 cm^{-1}, associated with the OH stretch of physically/chemically sorbed water, organic hydroxide groups or mineral hydroxide phases. This band was much less pronounced for the materials treated at higher calcination temperatures, as a result of increased NOM decomposition and mineral dehydration (Fig. 2a). From 300 °C onwards, bands around 1640 cm^{-1} (aromatic alkene and complexed carbonyl double-bonded carbon with oxygen) and 1400 cm^{-1} (symmetrical stretching of COO– or CO– groups of phenolic compounds) became less pronounced, due to the increased loss of NOM with increasing temperature. This was also confirmed by the TGA-MS signal for CO_2 formation (Fig. 2a). The band at 1040 cm^{-1}, attributed to the Si–O vibration, remained present over the whole temperature region, confirming the stability of the SiO_2 phase over the tested temperature range, as also shown with XRD. Finally, the band at 942 cm^{-1}, linked to stretching vibrations of Al–O, became less prominent with increasing temperature.

The effect of the calcination temperature on the physical properties of the granulated material was investigated (Table 1). The specific surface area (BET) strongly increased with the calcination temperature from 26.8 $m^2\ g^{-1}$ after drying at 100 °C to 316.1 $m^2\ g^{-1}$ after calcination at 400 °C. Above calcination temperatures of 400 °C, the specific surface area declined again. Firstly, the NOM degradation in the material, occurring between 200 °C–600 °C according to TGA-MS, increased the specific surface area by unblocking the pore network. Secondly, the enhanced crystallization of Al-phases at elevated temperatures

Table 1
The specific surface area (BET), density and crush strength of the obtained material after calcination of the granulated alum sludge at varying temperature.

Temperature	Specific surface area	Density	Crush strength
°C	$m^2\ g^{-1}$	$g\ cm^{-1}$	MPa
100	26.8	1.776 ± 0.010	7.194 ± 3.488
200	51.4	1.919 ± 0.005	1.997 ± 1.604
300	292.1	2.344 ± 0.002	2.596 ± 1.712
400	316.1	2.491 ± 0.003	4.530 ± 1.782
500	295.0	2.476 ± 0.001	7.881 ± 8.164
550	256.1	2.643 ± 0.003	7.839 ± 5.656
600	170.4	2.540 ± 0.001	7.733 ± 4.002

decreased the specific surface area (Jeon et al., 2018). Likely, a combination of these two mechanisms accounted for the recorded trend of the specific surface area with the calcination temperature. The material density also increased initially with increasing calcination temperature, reaching a maximum density of 2.643 g cm^{-1} at 550 °C. This increase in density with temperature was likely associated with the loss of NOM, which has a low specific weight. Most of the NOM decomposed at a temperature below 600 °C, according to the TGA-MS results, which likely explained why the measured density did not further increase after 550 °C. Finally, for the crush strength of the ABA granules dried at 100 °C, a relatively high value of 7.194 MPa was obtained. Increasing the calcination temperature to 200 °C resulted in a significant drop in the crushing strength. This was likely the result of i) the decomposition of organic matter (Fig. 2a), that acted as a binder between the mineral components of the sludge, and ii) the loss of the structural properties of this binder at increased temperature. The crushing strength strongly increased again for granules treated at 500 °C or higher, as the phase transition of γ-AlOOH to γ-Al_2O_3 affected the microstructure of the material (Tantawy, 2015).

The SEM micrograph of the ABA-550 material clearly showed the presence of Si-rich frustules of centric diatoms (Figure S2), which reached a size of up to 30 μm in diameter. The EDX elemental maps of Si suggested this biogenic Si accounts for a majority of Si in this material. Strong associations were observed between the appearance of Al and O in the material, confirming the presence of a prominent Al oxide phase (γ-Al_2O_3). Also an association between Ca, Cl and S was shown, suggesting the presence of $CaSO_4$ and $CaCl_2$. Next to the SEM micrographs, also an optical picture of the material was included (Figure S3). Using the granule size distribution of the ABA-550 material (Figure S4) and the simplified transfer function derived by Canga et al. (2014), it was possible to estimate the hydraulic conductivity of the granules in a filter system based on the D_{20} and D_{50}:

$$\log(K_{sat}) = 4.66 + 0.63 \times logD_{20} + 0.94 \times logD_{50} \quad (6)$$

with D_{20} equal to 1.2 mm, D_{50} equal to 1.8 mm and a resulting K_{sat} value of 89,092 cm s^{-1}.

3.3. P adsorption experiments

3.3.1. Adsorption capacity

The P adsorption properties of ABA-100, ABA-300 and ABA-550 were tested in 33 mg-P L^{-1} solutions with an initial pH ranging between 4 and 9 (Fig. 3a). At all tested pH values, the P adsorption of ABA-550 was higher than that of ABA-100 and ABA-300, while only limited differences in P adsorption were obtained between ABA-100 and ABA-300. The reason for the superior P adsorption on ABA-550 was twofold. Firstly, NOM had been removed from the ABA-550 material, whereas ABA materials treated at calcination temperatures of 300 °C or lower retained their high organic matter content. Carboxylate groups of NOM (*e.g.* humic substances) also interact with Al-oxyhydroxide surfaces, thereby strongly competing with inorganic anions (*e.g.* phosphate, arsenate) for inner-sphere sorption (Matilainen et al., 2010). Since the ABA materials treated at low calcination temperatures retained a high organic matter content, the Al-oxyhydroxide surfaces of these materials remained saturated with NOM (Jeon et al., 2018). This likely limited the P adsorption of ABA-100 and ABA-300 in comparison with that of ABA-550. Secondly, the different mineralogy of Al in these three ABA materials also influenced their P adsorption. The γ-Al_2O_3 phase, the main Al-phase in the ABA-550 material, has a higher P adsorption capacity than boehmite, the main Al-phase in the ABA-100 and ABA-300 materials, as proven by Li et al. (2013) at pH 5. It should be noted that the differences between the specific surface areas of the ABA materials likely had only a minor effect on P adsorption.

For the ABA-550 material, a clear decrease in P adsorption was shown with the increase in the initial pH of the adsorption solution (Fig. 3a), with a P adsorption of 2.02 mg-P g^{-1} at pH 4 and only 1.24 mg-P g^{-1} at pH 9. Especially from pH 7 onwards, the P adsorption diminished clearly. The explanation for this could be found in the P sorption mechanism on ABA-550, which could be approached as P sorption on γ-Al_2O_3 alone, since i) this phase was the most prominent in ABA-550, ii) P sorption on quartz, the second main phase in the ABA materials (Table S1), is negligible (Del Bubba et al., 2003) and iii) the study of He et al. showed a very similar decrease in P adsorption on γ-Al_2O_3 as a function of the solution pH (He et al., 1997). In general, the pH dependency of P sorption on Al-oxyhydroxide surfaces is determined by i) the aqueous P speciation, which here ranged from a $H_2PO_4^-$ dominant to a HPO_4^{2-} dominant system with the pH ranging from 4 to 9 (pK_{a2} of phosphoric acid is 7.20) (Everaert et al., 2019), and ii) the charge of the γ-Al_2O_3 surface as a result of the (de)protonation of the surface hydroxyl groups, which ranges from positive to slightly negative with the pH ranging from 4 to 9 (pzc of γ-Al_2O_3 at 25 °C is 7.5) (Mustafa et al., 1998). The relatively low P adsorption obtained in alkaline P solutions was likely caused by the electrostatic repulsion that occurred between the HPO_4^{2-} anions in solution and the negatively charged γ-Al_2O_3 surface, which prevents inner-sphere P complexation. This hypothesis is supported by the fact that the P adsorption clearly dropped when the pH of

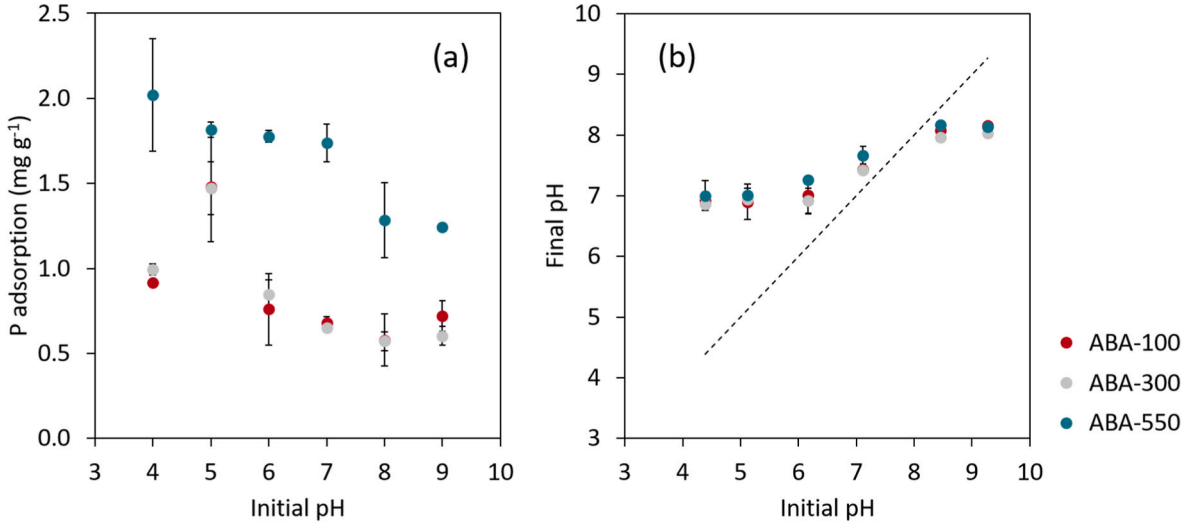

Fig. 3. The P adsorption by materials ABA-100, ABA-300 and ABA-550 after 24 h incubation as a function of the initial solution pH (a) and the final solution pH as a function of the initial solution pH (b). Error bars represent standard deviation (n = 2).

the synthetic P solutions surpassed both the pzc value of γ-Al_2O_3 and the pK_{a2} value of phosphoric acid, which both contributed to a stronger repulsion. For the ABA-100 material and ABA-300 materials, the obtained trend in P adsorption with changing solution pH was comparable with the trend obtained for untreated alum sludge materials in previous studies (Kim et al., 2002; Maqbool et al., 2016; Yang et al., 2006b).

In the case of the acid and alkaline synthetic P solutions, the initial pH values clearly deviated from the final pH values (Fig. 3b), which both equilibrated around pH 7. Again, the P adsorption mechanism of γ-Al_2O_3 could explain these effects. Using ATR-FTIR, Zheng et al. (2012) investigated the speciation of adsorbed P on γ-Al_2O_3 in a system at pH 4 and pH 9. At pH 4, the diprotonated monodentate inner-sphere complex was the main P speciation on the strongly positively charged alumina surface, while at pH 9 both non-protonated bidentate binuclear complexes and monoprotonated monodentate complexes were present. This means that incubating the ABA-550 material in the P solution of pH 4 removed $H_2PO_4^-$ from the solution and protons were captured by the surface hydroxyl groups, which increased the pH; incubating the ABA-550 material in a P solution of pH 9 removed HPO_4^{2-} from the solution, which decreased the pH.

Because of the superior P adsorption properties of ABA-550, the P adsorption isotherm of this material was determined at pH 7 (Fig. 4). The Langmuir and Freundlich isotherm models were used to describe the P adsorption results at equilibrium (Table 2). Using the Langmuir model, a maximum adsorption P capacity of 7.27 mg-P g^{-1} (0.235 mmol g^{-1}) was derived. This P adsorption capacity was lower than reported capacities for powdered alum sludge at pH 7, *e.g.* 23.0 mg-P g^{-1} reported by Babatunde and Zhao (2010) and 14.9 mg-P g^{-1} reported by Yang et al. (2008). It is likely that the granulation of the alum sludge, which is necessary for the use of ABA in filter beds, caused a decrease in the adsorption capacity by making a fraction of the P sorption sites less accessible (Li et al., 2018). It should also be noted that the change in solution pH during the adsorption reaction was not significant for the isotherm solutions, which was in line with the previous results on P adsorption at pH 7 (Fig. 3a). A higher correlation coefficient was obtained for the Freundlich model (0.960) compared to the Langmuir model (0.906) (Table 2). The study by Zheng et al. (2012) showed that, in general, P sorption on γ-Al_2O_3 at lower P concentrations can be described by the Langmuir model, whereas the Freundlich model can be applied to a broader range of P concentrations.

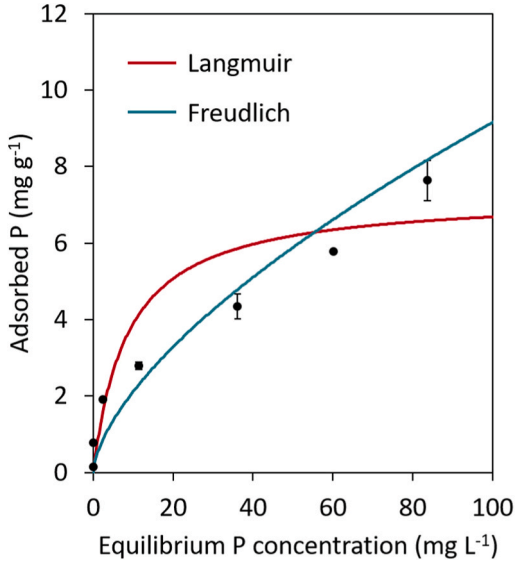

Fig. 4. The P adsorption isotherm of the ABA-550 material, determined at 25 °C after 24 h incubation. Error bars represent standard deviation (n = 2).

Table 2
Adsorption isotherm parameters of the P adsorption on the ABA-550 material, according to the Langmuir model and the Freundlich model.

Langmuir			Freundlich		
$q_{m,\ cal}$	k_L	r^2	N	k_F	r^2
mg-P g^{-1}		-	-	*L* g^{-1}	-
7.27	0.12	0.91	2.632	1.24	0.96

3.3.2. P adsorption kinetics of ABA-550

3.3.2.1. Effect of S:L ratio. The effect of the solid to liquid ratio (S:L) on P removal is important for determining the required amount of ABA-550 material to remediate water within a certain reaction time. Here, a higher S:L ratio resulted in a faster decrease in the P concentration in solution as a function of time (Fig. 5a). Adsorption for 60 min at a S:L ratio of 50 g L^{-1} removed all P from the solution, while this was not the case for 2 or 10 g L^{-1} loadings. On a weight basis, however, the P adsorption as a function of time was comparable among the S:L ratios (Fig. 5b). The maximum P loading of the ABA-550 material of ~0.07 mg-P g^{-1} was obtained at 2 g L^{-1} and 10 g L^{-1}. The adsorption kinetics associated with the use of different S:L ratios were examined by fitting the adsorption data to the pseudo-first-order, pseudo-second-order and intra-particle diffusion models (Table 3). The k_1 and k_2 values increased with increasing S:L ratio, while the q_e values increased with decreasing S:L ratio. When comparing the k and q_e values at 50 g L^{-1} with those reported earlier for powdered uncalcined sludge, k_1 and k_2 were higher for the calcined granular ABA-550, whereas the q_e values were higher for the powdered uncalcined sludge (Babatunde and Zhao, 2010). The higher rate constant of the ABA-550 material were likely attributed to changes in the microstructure of the material and crystallization of the Al phases, associated with sludge calcination, while the higher q_e values of the uncalcined sludge were the result of a higher P adsorption capacity of that specific uncalcined sludge material (23.0 mg-P g^{-1}) compared to that of ABA-550 (7.27 mg-P g^{-1}) at pH 7 (Langmuir model parameter). From the intra-particle diffusion model, it was found that the intra-particle diffusion rate constant k_d increased slightly with decreasing S:L ratio. The study of Babatunde and Zhao (2010) suggested that, at a constant S:L ratio, intra-particle diffusion is a predominant mechanism for P adsorption at a high initial P concentration. Comparing this aspect to the setup of this study with a varying S:L ratio and constant initial P concentration, it was also shown that at a higher P exposure (low S:L ratio) the intra-particle diffusion rate constant k_d is slightly higher than at a lower P exposure (high S:L ratio). Nevertheless, this influence remained limited in these conditions since, for all tested S:L ratios, the ABA-550 material was performing far below its maximum adsorption capacity of 7.27 mg-P g^{-1}. Finally, while the 50 g L^{-1} loading was able to remove all P within 60 min of incubation, the P removal efficiency was only 41% at 10 g L^{-1} and 9% at 2 g L^{-1} after 120 min of incubation (Fig. 5c).

3.4. Effect of granule size

The particle size of granular sorbents can affect the adsorption kinetics due to the effect of intra-particle diffusion limitations. The particle size distribution of the ABA-550 material showed that 13% of the material had a particle size <1 mm, 51% had a particle size between 1 and 2 mm and 36% had a particle size between 2 and 4 mm (Figure S4). For these different size fractions of the ABA-550 material, a smaller particle size resulted in a faster decrease of the P concentration in solution as a function of time, which is in agreement with the trend obtained by Yang et al. (2006a) for uncalcined material. Yet, differences between the 1–2 mm and the 2–4 mm size fractions remained relatively small (Fig. 6a). A comparison of the P adsorption of these different size fractions on a weight basis showed that the particle size did affect the P adsorption kinetics (Fig. 6b). This was also confirmed by the large

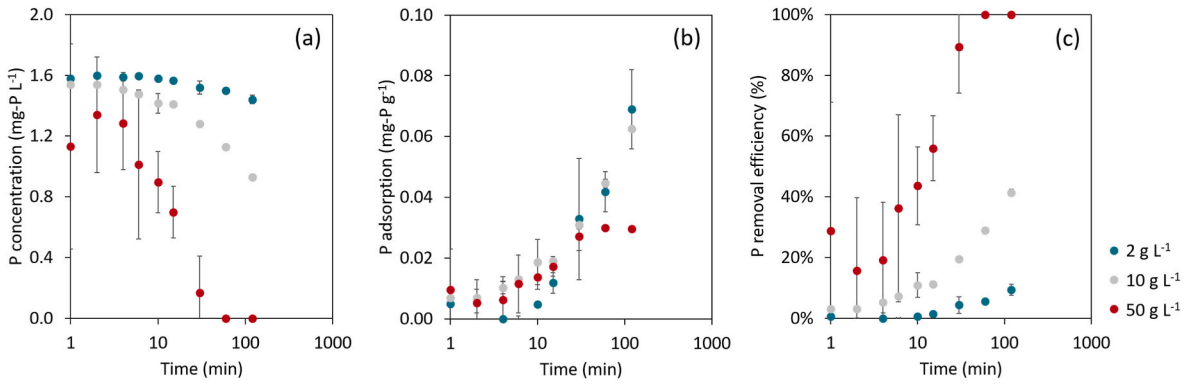

Fig. 5. The P adsorption kinetics of the ABA-550 material at different S:L ratio (2 g L^{-1}, 10 g L^{-1} and 50 g L^{-1}), presented by the P concentration (a), the P adsorption (b) and the P removal efficiency (c) as a function of the incubation time. Error bars represent standard deviation (n = 2).

Table 3
Kinetic parameter values of the P adsorption on the ABA-550 material at varying S:L ratio and varying particle size.

		S:L ratio (g L^{-1})			Size (mm)		
		2	10	50	<1	1–2	2–4
Pseudo-first-order	$q_{e1,cal}$ (mg-P g^{-1})	0.070	0.057	0.020	0.313	0.098	0.070
	k_1 (min^{-1})	0.039	0.045	0.130	0.045	0.035	0.031
	r^2 (–)	0.89	0.98	0.99	0.94	0.96	0.94
Pseudo-second-order	$q_{e2,cal}$ (mg-P g^{-1})	0.144	0.060	0.032	0.405	0.116	0.108
	k_2 (g mg-P^{-1} min^{-1})	0.049	0.708	5.857	0.080	0.143	0.365
	r^2 (–)	0.20	0.93	0.97	0.87	0.37	0.78
Intra-particle diffusion	k_d (mg-P g^{-1} $min^{-1/2}$)	0.007	0.006	0.002	0.03	0.009	0.006
	r^2 (–)	0.92	0.99	0.89	0.94	0.96	0.89

difference in the calculated rate constants between the <1 mm fraction on the one hand, and the 1–2 mm and the 2–4 mm fractions on the other hand (Table 3). The r^2 value of the pseudo-first-order model was much higher compared to that of the pseudo-second-order model, causing the interpretation to be focused on the pseudo-first-order model observations. This showed a decrease in the rate constant and the q_e value with increasing particle size. The intra-particle diffusion rate constant k_d strongly decreased with increasing particle size. This could be explained by the fact that the <1 mm material had a significantly higher external surface area compared to the 1–2 mm and the 2–4 mm size fractions. A larger particle size (1–2 mm, 2–4 mm) would require P to diffuse significantly longer within a single ABA-particle to access internal bonding sites, making intra-particle diffusion a more pronounced rate-limiting step compared to the finer <1 mm material. Finally, the P adsorption efficiency was also very different between the different size fractions after 120 min, ranging from 5% for the 2–4 mm fraction to 47% for the <1 mm fraction (Fig. 6c).

3.5. Pilot-scale column test

To test the performance of both the ABA-100 and the ABA-550 materials as an adsorbent in a water treatment installation, a pilot-scale adsorption column was used for the treatment of surface water with a P concentration of 0.47 mg-P L^{-1} at the set flow rate of 200 L h^{-1}. The ABA-100 material, on the one hand, started to disintegrate after contact with water. As a result, the granules were not visible anymore after a few hours of incubation, and fine ABA-100 material was flushed out of the column (Figure S5). The use of untreated alum sludge in powder form in this column would likely cause comparable issues. The adsorption column with ABA-550 material, on the other hand, showed no problems regarding granule stability, which resulted in a performant percolation throughout the experiment. This clearly illustrated that the stability of the sludge granules throughout a column adsorption treatment is a key factor for application, and that granule stability was warranted by the calcination process. Furthermore, the column with ABA-550 material was able to significantly reduce the P concentration (Fig. 7). The P removal efficiency always exceeded 86%, thereby obtaining an average effluent P concentration of 0.035 mg-P L^{-1}. The obtained effluent P concentration was very close to 0.033 mg-P L^{-1}, which is considered the target P concentration for the replenishment of the water basin. The surface water treatment also slightly affected the pH and the turbidity of

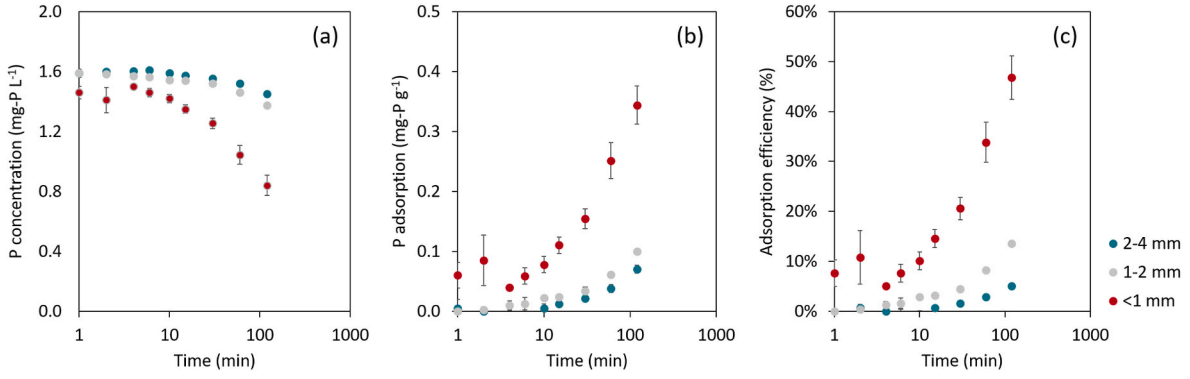

Fig. 6. The P adsorption kinetics by different size fraction of the ABA-550 material (<1 mm, 1–2 mm, 2–4 mm) at S:L ratio of 2 g L^{-1}, presented by the P concentration (a), the P adsorption (b) and the P removal efficiency (c) as a function of incubation time. Error bars represent standard deviation (n = 2).

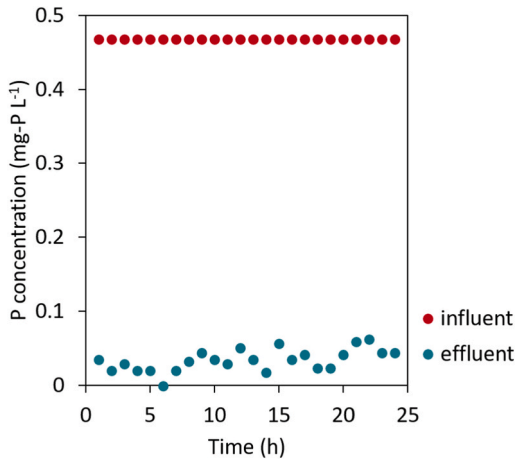

Fig. 7. The P concentration at the inlet and the outlet of the pilot-scale adsorption column.

the water, although these effects stabilized towards the end of the 24 h-treatment period (Figure S6). During the test, the turbidity of the effluent decreased from 3.3 NTU to minimum 1.6 NTU, which suggested that a fraction of colloidal material in the water could be maintained by the ABA-550 filter. The pH of the treated water increased from 7.6 to maximum 8.1 during the treatment. This slight alkaline effect of ABA-550 was also obtained in the lab-scale tests with synthetic P solutions of pH 7 (Fig. 3b). With this pilot-scale adsorption experiment, the ABA-550 material was proven capable of performing in a column system and can therefore be applied in industrial-size adsorption systems in the future.

4. Conclusions

This study examined the calcination of granular alum sludge material, aiming to develop a performant P adsorbent for use in column water treatment systems. For the range of tested calcination temperatures, material characterization and P adsorption testing indicated that the granular material calcined at 550 °C was the most promising. The obtained material from this granulation and calcination (ABA-550 material) showed a maximum P adsorption capacity of 7.27 mg-P g^{-1}. Compared to the fine-grained, fresh alum sludge, the overall adsorption capacity was slightly reduced, which was likely the result of the reduction of surface area with granulation. However, the ABA-550 material showed, next to its satisfactory P adsorption capacity, also the required structural integrity, which warranted its suitability for larger-scale application. Finally, a pilot-scale adsorption column test showed that the ABA-550 material was successful in the P removal from a P-rich surface water stream at a flow rate of 200 L h^{-1}, as a P removal efficiency >86% was maintained throughout the experiment. Based on the findings of this study, future research can further explore the capabilities of calcined ABA adsorbents in column systems, either at pilot-scale or industrial scale. Also the regeneration potential of saturated ABA adsorbents can be investigated, in order to reuse the adsorbent and recycle the captured P.

CRediT author statement

Maarten Everaert: Formal analysis, Validation, Writing - Original Draft, Writing - Review & Editing, Visualization; **Jef Bergmans**: Validation, Investigation, Writing - Review & Editing, Conceptualization; **Kris Broos**: Supervision, Funding acquisition, Writing - Review & Editing; **Benjamin Hermans**: Investigation, Resources, Writing - Review & Editing; **Bart Michielsen**: Validation, Investigation, Writing - Review & Editing, Supervision, Conceptualization.

Declaration of competing interest

The authors declare that they have no known competing financial interests or personal relationships that could have appeared to influence the work reported in this paper.

Acknowledgments

This work was supported by the Interreg North Sea Region project on nutrient recovery from agricultural waters, NuReDrain (grant number 38-2-17-16). Also, the authors would like to thank Sten Janssen for the alum sludge handling, Evelyn Moens for the lab-scale adsorption experiments, Veerle D'Haeseleer and Janus Van Massenhove for the pilot-scale adsorption experiment, Myrjam Mertens for XRD analysis, Raymond Kemps for SEM-EDX, Danny Havermans for mechanical testing and Annemarie De Wilde for N_2 sorption, TGA-MS and He pycnometry.

Appendix A. Supplementary data

Supplementary data to this article can be found online at https://doi.org/10.1016/j.jenvman.2020.111525.

References

Ahmad, T., Ahmad, K., Alam, M., 2016. Sustainable management of water treatment sludge through 3'R' concept. J. Clean. Prod. 124, 1–13. https://doi.org/10.1016/j.jclepro.2016.02.073.

Babatunde, A.O., Zhao, Y.Q., 2010. Equilibrium and kinetic analysis of phosphorus adsorption from aqueous solution using waste alum sludge. J. Hazard Mater. 184, 746–752. https://doi.org/10.1016/j.jhazmat.2010.08.102.

Babatunde, A.O., Zhao, Y.Q., Yang, Y., Kearney, P., 2008. Reuse of dewatered aluminium-coagulated water treatment residual to immobilize phosphorus: batch and column trials using a condensed phosphate. Chem. Eng. J. 136, 108–115. https://doi.org/10.1016/j.cej.2007.03.013.

Babatunde, A.O., Zhao, Y.Q., Zhao, X.H., 2010. Alum sludge-based constructed wetland system for enhanced removal of P and OM from wastewater: concept, design and performance analysis. Bioresour. Technol. 101, 6576–6579. https://doi.org/10.1016/j.biortech.2010.03.066.

Canga, E., Iversen, B.V., Kjaergaard, C., 2014. A simplified transfer function for estimating saturated hydraulic conductivity of porous drainage filters. Water Air Soil Pollut. 225 https://doi.org/10.1007/s11270-013-1794-8.

Carpenter, S.R., 2008. Phosphorus control is critical to mitigating eutrophication. Proc. Natl. Acad. Sci. U.S.A. 105, 11039–11040. https://doi.org/10.1073/pnas.0806112105.

Cheng, G., Li, Q., Su, Z., Sheng, S., Fu, J., 2018. Preparation, optimization, and application of sustainable ceramsite substrate from coal fly ash/waterworks sludge/oyster shell for phosphorus immobilization in constructed wetlands. J. Clean. Prod. 175, 572–581. https://doi.org/10.1016/j.jclepro.2017.12.102.

Dassanayake, K.B., Jayasinghe, G.Y., Surapaneni, A., Hetherington, C., 2015. A review on alum sludge reuse with special reference to agricultural applications and future challenges. Waste Manag. 38, 321–335. https://doi.org/10.1016/j.wasman.2014.11.025.

Dayton, E.A., Basta, N.T., 2005. A method for determining the phosphorus sorption capacity and amorphous aluminum of aluminum-based drinking water treatment residuals. J. Environ. Qual. 34, 1112–1118. https://doi.org/10.2134/jeq2004.0230.

Del Bubba, M., Arias, C.A., Brix, H., 2003. Phosphorus adsorption maximum of sands for use as media in subsurface flow constructed reed beds as measured by the Langmuir isotherm. Water Res. 37, 3390–3400. https://doi.org/10.1016/S0043-1354(03)00231-8.

Desmidt, E., Ghyselbrecht, K., Zhang, Y., Pinoy, L., Van Der Bruggen, B., Verstraete, W., Rabaey, K., Meesschaert, B., 2015. Global phosphorus scarcity and full-scale P-recovery techniques: a review. Crit. Rev. Environ. Sci. Technol. 45, 336–384. https://doi.org/10.1080/10643389.2013.866531.

Djodjic, F., Börling, K., Bergström, L., 2004. Phosphorus leaching in relation to soil type and soil phosphorus content. J. Environ. Qual. 33, 678–684. https://doi.org/10.2134/jeq2004.6780.

Dox, K., Everaert, M., Merckx, R., Smolders, E., 2019. Optimization of phosphate recovery from urine by layered double hydroxides. Sci. Total Environ. 682, 437–446. https://doi.org/10.1016/j.scitotenv.2019.05.181.

Everaert, M., Dox, K., Steele, J.A., De Vos, D., Smolders, E., 2019. Solid-state speciation of interlayer anions in layered double hydroxides. J. Colloid Interface Sci. 537, 151–162. https://doi.org/10.1016/j.jcis.2018.11.010.

Freundlich, H., Hatfield, H.S., 1926. Colloid and Capillary Chemistry. Methuen And Co. Ltd, London, UK.

Georgantas, D.A., Grigoropoulou, H.P., 2005. Phosphorus removal from synthetic and municipal wastewater using spent alum sludge. Water Sci. Technol. 52, 525–532.

Guo, F., Wu, F., Mu, Y., Hu, Y., Zhao, X., Meng, W., Giesy, J.P., Lin, Y., 2016. Characterization of organic matter of plants from lakes by thermal analysis in a N2 atmosphere. Sci. Rep. 6, 1–7. https://doi.org/10.1038/srep22877.

He, L.M., Zelazny, L.W., Baligar, V.C., Ritchey, K.D., Martens, D.C., 1997. Ionic strength effects on sulfate and phosphate adsorption on γ-alumina and kaolinite: triple-layer model. Soil Sci. Soc. Am. J. 61, 784–793. https://doi.org/10.2136/sssaj1997.03615995006100030011x.

Hovsepyan, A., Bonzongo, J.C.J., 2009. Aluminum drinking water treatment residuals (Al-WTRs) as sorbent for mercury: implications for soil remediation. J. Hazard Mater. 164, 73–80. https://doi.org/10.1016/j.jhazmat.2008.07.121.

Ippolito, J.A., Scheckel, K.G., Barbarick, K.A., 2009. Selenium adsorption to aluminum-based water treatment residuals. J. Colloid Interface Sci. 338, 48–55. https://doi.org/10.1016/j.jcis.2009.06.023.

Jeon, E.K., Ryu, S., Park, S.W., Wang, L., Tsang, D.C.W., Baek, K., 2018. Enhanced adsorption of arsenic onto alum sludge modified by calcination. J. Clean. Prod. 176, 54–62. https://doi.org/10.1016/j.jclepro.2017.12.153.

Jung, K.W., Hwang, M.J., Jeong, T.U., Chau, D.M., Kim, K., Ahn, K.H., 2016. Entrapment of powdered drinking water treatment residues in calcium-alginate beads for fluoride removal from actual industrial wastewater. J. Ind. Eng. Chem. 39, 101–111. https://doi.org/10.1016/j.jiec.2016.05.017.

Kang, S., Park, S.M., Park, J.G., Baek, K., 2019. Enhanced adsorption of arsenic using calcined alginate bead containing alum sludge from water treatment facilities. J. Environ. Manag. 234, 181–188. https://doi.org/10.1016/j.jenvman.2018.12.105.

Kim, J.G., Kim, J.H., Moon, H.S., Chon, C.M., Ahn, J.S., 2002. Removal capacity of water plant alum sludge for phosphorus in aqueous solutions. Chem. Speciat. Bioavailab. 14, 67–73. https://doi.org/10.3184/095422902782775344.

Kim, Y.S., Kim, D.H., Yang, J.S., Baek, K., 2012. Adsorption characteristics of as(III) and as(V) on alum sludge from water purification facilities. Separ. Sci. Technol. 47, 2211–2217. https://doi.org/10.1080/01496395.2012.700676.

Kim, J.G., Kim, H. Bin, Yoon, G.S., Kim, S.H., Min, S.J., Tsang, D.C.W., Baek, K., 2020. Simultaneous oxidation and adsorption of arsenic by one-step fabrication of alum sludge and graphitic carbon nitride (g-C3N4). J. Hazard Mater. 383, 121138. https://doi.org/10.1016/j.jhazmat.2019.121138.

Kizito, S., Luo, H., Wu, S., Ajmal, Z., Lv, T., Dong, R., 2017. Phosphate recovery from liquid fraction of anaerobic digestate using four slow pyrolyzed biochars: dynamics of adsorption, desorption and regeneration. J. Environ. Manag. 201, 260–267. https://doi.org/10.1016/j.jenvman.2017.06.057.

Kumar, P.S., Korving, L., van Loosdrecht, M.C.M., Witkamp, G.J., 2019. Adsorption as a technology to achieve ultra-low concentrations of phosphate: research gaps and economic analysis. Water Res. X 4, 100029. https://doi.org/10.1016/j.wroa.2019.100029.

Langmuir, I., 1932. Vapor pressures, evaporation, condensation and adsorption. J. Am. Chem. Soc. 54, 2798–2832. https://doi.org/10.1021/ja01346a022.

Levin, Igor, Brandon, David, 1998. Metastable alumina polymorphs: crystal structures and transition sequences. J. Am. Ceram. Soc. 81, 1995–2012.

Li, W., Feng, X., Yan, Y., Sparks, D.L., Phillips, B.L., 2013. Solid-state NMR spectroscopic study of phosphate sorption mechanisms on aluminum (hydr)oxides. Environ. Sci. Technol. 47, 8308–8315. https://doi.org/10.1021/es400874s.

Li, X., Cui, J., Pei, Y., 2018. Granulation of drinking water treatment residuals as applicable media for phosphorus removal. J. Environ. Manag. 213, 36–46. https://doi.org/10.1016/j.jenvman.2018.02.056.

Liu, R., Zhao, Y., Sibille, C., Ren, B., 2016. Evaluation of natural organic matter release from alum sludge reuse in wastewater treatment and its role in P adsorption. Chem. Eng. J. 302, 120–127. https://doi.org/10.1016/j.cej.2016.05.019.

Maqbool, N., Khan, Z., Asghar, A., 2016. Reuse of alum sludge for phosphorus removal from municipal wastewater. Desalin. Water Treat. 57, 13246–13254. https://doi.org/10.1080/19443994.2015.1055806.

Matilainen, A., Vepsäläinen, M., Sillanpää, M., 2010. Natural organic matter removal by coagulation during drinking water treatment: a review. Adv. Colloid Interface Sci. 159, 189–197. https://doi.org/10.1016/j.cis.2010.06.007.

Mcdowell, R.W., Sharpley, A.N., Condron, L.M., Haygarth, P.M., Brookes, P.C., 2001. Processes controlling soil phosphorus release to runoff and implications for agricultural management. Nutrient Cycl. Agroecosyst. 59, 269–284. https://doi.org/10.1023/A:1014419206761.

Mustafa, S., Dilara, B., Neelofer, Z., Naeem, A., Tasleem, S., 1998. Temperature effect on the surface charge properties of γ-Al2O3. J. Colloid Interface Sci. 204, 284–293. https://doi.org/10.1006/jcis.1998.5572.

Seftel, E.M., Ciocarlan, R.G., Michielsen, B., Meynen, V., Mullens, S., Cool, P., 2018. Insights into phosphate adsorption behavior on structurally modified ZnAl layered double hydroxides. Appl. Clay Sci. 165, 234–246. https://doi.org/10.1016/j.clay.2018.08.018.

Shen, C., Zhao, Y., Liu, R., 2018. Development of pellet-type adsorbent based on water treatment residual. Desalin. Water Treat. 112, 3–11. https://doi.org/10.5004/dwt.2018.21997.

Sujana, M.G., Thakur, R.S., Rao, S.B., 1998. Removal of fluoride from aqueous solution by using alum sludge. J. Colloid Interface Sci. 206, 94–101. https://doi.org/10.1006/jcis.1998.5611.

Tantawy, M.A., 2015. Characterization and pozzolanic properties of calcined alum sludge. Mater. Res. Bull. 61, 415–421. https://doi.org/10.1016/j.materresbull.2014.10.042.

Tie, J., Chen, D., Wan, Y., Yan, C., Zhang, X., 2013. Adsorption removal of phosphorus from aqueous solution by heat-activated alum sludge. Asian J. Chem. 25, 9129–9134. https://doi.org/10.14233/ajchem.2013.15040.

Wang, C., Guo, W., Tian, B., Pei, Y., Zhang, K., 2011. Characteristics and kinetics of phosphate adsorption on dewatered ferric-alum residuals. J. Environ. Sci. Heal. - Part A Toxic/Hazardous Subst. Environ. Eng. 46, 1632–1639. https://doi.org/10.1080/10934529.2011.623643.

Xu, G.R., Zou, J.L., Li, G.B., 2008. Effect of sintering temperature on the characteristics of sludge ceramsite. J. Hazard Mater. 150, 394–400. https://doi.org/10.1016/j.jhazmat.2007.04.121.

Yang, Y., Tomlinson, D., Kennedy, S., Zhao, Y.Q., 2006a. Dewatered alum sludge: a potential adsorbent for phosphorus removal. Water Sci. Technol. 54, 207–213. https://doi.org/10.2166/wst.2006.564.

Yang, Y., Zhao, Y.Q., Babatunde, A.O., Wang, L., Ren, Y.X., Han, Y., 2006b. Characteristics and mechanisms of phosphate adsorption on dewatered alum sludge. Separ. Purif. Technol. 51, 193–200. https://doi.org/10.1016/j.seppur.2006.01.013.

Yang, Y., Zhao, Y.Q., Kearney, P., 2008. Influence of ageing on the structure and phosphate adsorption capacity of dewatered alum sludge. Chem. Eng. J. 145, 276–284. https://doi.org/10.1016/j.cej.2008.04.026.

Yang, M., Lin, J., Zhan, Y., Zhu, Z., Zhang, H., 2015. Immobilization of phosphorus from water and sediment using zirconium-modified zeolites. Environ. Sci. Pollut. Res. 22, 3606–3619. https://doi.org/10.1007/s11356-014-3604-2.

Yoon, S.Y., Lee, C.G., Park, J.A., Kim, J.H., Kim, S.B., Lee, S.H., Choi, J.W., 2014. Kinetic, equilibrium and thermodynamic studies for phosphate adsorption to magnetic iron oxide nanoparticles. Chem. Eng. J. 236, 341–347. https://doi.org/10.1016/j.cej.2013.09.053.

Zhao, X.H., Zhao, Y.Q., 2009. Investigation of phosphorus desorption from P-saturated alum sludge used as a substrate in constructed wetland. Separ. Purif. Technol. 66, 71–75. https://doi.org/10.1016/j.seppur.2008.11.020.

Zheng, T.T., Sun, Z.X., Yang, X.F., Holmgren, A., 2012. Sorption of phosphate onto mesoporous γ-alumina studied with in-situ ATR-FTIR spectroscopy. Chem. Cent. J. 6, 1–10. https://doi.org/10.1186/1752-153X-6-26.

Zhou, Y., Haynes, R.J., 2011. Removal of Pb (II), Cr (III) and Cr (VI) from Aqueous Solutions Using Alum-Derived Water Treatment Sludge 631–643. https://doi.org/10.1007/s11270-010-0505-y.

Zohar, I., Ippolito, J.A., Massey, M.S., Litaor, I.M., 2017. Innovative approach for recycling phosphorous from agro-wastewaters using water treatment residuals (WTR). Chemosphere 168, 234–243. https://doi.org/10.1016/j.chemosphere.2016.10.041.